Origin of hydrophobicity and enhanced water hydrogen bond strength near purely hydrophobic solutes

Joze Grdadolnik[a], Franci Merzel[a], and Franc Avbelj[a,1]

[a]Department of Biomolecular Structure, National Institute of Chemistry, SI 1000 Ljubljana, Slovenia

Edited by H. Eugene Stanley, Boston University, Boston, MA, and approved November 28, 2016 (received for review August 4, 2016)

Hydrophobicity plays an important role in numerous physicochemical processes from the process of dissolution in water to protein folding, but its origin at the fundamental level is still unclear. The classical view of hydrophobic hydration is that, in the presence of a hydrophobic solute, water forms transient microscopic "icebergs" arising from strengthened water hydrogen bonding, but there is no experimental evidence for enhanced hydrogen bonding and/or icebergs in such solutions. Here, we have used the redshifts and line shapes of the isotopically decoupled IR oxygen–deuterium (O-D) stretching mode of HDO water near small purely hydrophobic solutes (methane, ethane, krypton, and xenon) to study hydrophobicity at the most fundamental level. We present unequivocal and model-free experimental proof for the presence of strengthened water hydrogen bonds near four hydrophobic solutes, matching those in ice and clathrates. The water molecules involved in the enhanced hydrogen bonds display extensive structural ordering resembling that in clathrates. The number of ice-like hydrogen bonds is 10–15 per methane molecule. Ab initio molecular dynamics simulations have confirmed that water molecules in the vicinity of methane form stronger, more numerous, and more tetrahedrally oriented hydrogen bonds than those in bulk water and that their mobility is restricted. We show the absence of intercalating water molecules that cause the electrostatic screening (shielding) of hydrogen bonds in bulk water as the critical element for the enhanced hydrogen bonding around a hydrophobic solute. Our results confirm the classical view of hydrophobic hydration.

hydrophobic hydration | hydrogen bonding | IR spectroscopy | electrostatic screening | ab initio molecular dynamics

Despite its great importance in numerous phenomena, the origin of hydrophobicity remains one of the most disputed topics in science (1–5). Experimental studies have shown that small purely hydrophobic solutes (alkanes and noble gases) in water increase the order (6, 7) and restrict the mobility (8) of neighboring water molecules. There are several opposing views on how to explain these data. The classical view is that a solute modifies water structure by forming transient, semiordered clathrate-like clusters ("icebergs"; used here only as a loose term) around it, arising from enhanced water hydrogen bonding (H bonding) (6, 7). This enhancement is brought about by either strengthening (9) or increasing the number of water to water H bonds (10). The classical view explains the characteristic changes in the thermodynamic variables of hydrophobic hydration (positive ΔG, ΔC_p, negative ΔS, and ΔH) and the restricted mobility of water molecules observed by NMR (8). Neutron diffraction (11, 12) and extended X-ray absorption fine structure (EXAFS) (13) studies, however, show that the water molecules around small purely hydrophobic molecules do not differ significantly from those in pure liquid water. According to the dynamic view, the hydrophobic solute causes slowdown of the dynamics of the nearby water molecules by obstructing the jump mechanism of rotational relaxation, whereas water structure and H-bonding strength remain basically unchanged (5, 14). The main problem of these two views is that there is essentially no direct experimental support for enhanced H bonding and resulting formation of icebergs in the hydration shell of small purely hydrophobic solutes (15) or a jump mechanism of rotational relaxation of the water molecules (5). An alternative view, arguing that the characteristic changes in thermodynamic variables of hydrophobic hydration can be explained by the difficulty of a solute molecule to be accommodated in an appropriate cavity in water because of small size of the water molecules, was proposed by Lee (16). Baldwin (17) recently suggested that extensive ordering of water molecules in the hydration shell of hydrophobic molecules is caused by van der Waals attraction between hydrophobic C and water O atoms.

Experimental proof for strengthened water H bonds and icebergs near purely hydrophobic solutes (alkanes and noble gases) would confirm unequivocally the classical view. Vibrational spectroscopy of the oxygen–hydrogen (O-H) stretching mode (ν_{OH}) is commonly used as the most reliable, sensitive, and model-free approach for determining relative strengths of H bonds (18–24). Any frequency downshift (redshift) of the ν_{OH} mode, detected by comparing spectra of bulk water with those of the water molecules perturbed by solute, would indicate enhanced H-bond strength. Moreover, the spectral line width of ν_{OH} is commonly used to assess structural order: a narrower line width indicates greater structural order (23, 25). Measuring redshifts and line widths of the water molecules perturbed by hydrophobic solutes is very difficult because of the latter's very low solubility and further complicated by the formation of solid clathrates at the high pressures and low temperatures used to increase solubility. Vibrational spectra of the water molecules perturbed by small purely hydrophobic solutes have not been measured. However, the redshift of water ν_{OH} has been observed in the hydration shell of several amphipathic solutes at high concentrations (20–22, 24). These measurements are, however, not convincing proof of enhanced water H-bond strength near hydrophobic solutes, because polar parts of the molecules and concentration effects could affect the results considerably (14, 26). Here, we used the redshifts and line shapes of the isotopically

Significance

Hydrophobicity governs a wide range of fundamental physicochemical processes, but its physical origin is unclear. The classical explanation of hydrophobicity is that tiny "icebergs" are formed near such solutes; however, no experimental proof has been advanced for their existence. Here, we used four small purely hydrophobic solutes (methane, ethane, krypton, and xenon) in water to study hydrophobicity at the most fundamental level. We present unequivocal experimental proof for strengthened water hydrogen bonds near purely hydrophobic solutes, matching those in ice and clathrates. The water molecules involved in the enhanced hydrogen bonds display extensive structural ordering resembling that in clathrates, thus indicating the fundamental interconnection between electrostatic screening (shielding) and the hydrophobic effect.

Author contributions: J.G., F.M., and F.A. performed research, analyzed data, and wrote the paper.

The authors declare no conflict of interest.

This article is a PNAS Direct Submission.

Freely available online through the PNAS open access option.

[1]To whom correspondence should be addressed. Email: Franc.Avbelj@ki.si.

This article contains supporting information online at www.pnas.org/lookup/suppl/doi:10.1073/pnas.1612480114/-/DCSupplemental.

decoupled IR oxygen–deuterium (O-D) stretching mode (ν_{OD}) of four purely hydrophobic solutes in water together with ab initio molecular dynamics (MD) simulations of methane in water to study the origin of hydrophobicity at the most fundamental level.

Results and Discussion

IR Spectroscopy of Water Molecules in the Neighborhood of Purely Hydrophobic Solutes. The redshifts and line widths of the O-D stretching mode of the water molecules were measured when perturbed by small purely hydrophobic solutes: methane, ethane, krypton, and xenon. The very low solubility of these solutes in water was increased by using high pressure (14–56 bar) and low temperature (285–299 K). The schematic setup of the IR experiment is shown in *SI Appendix*, Fig. S1.

We focused on the decoupled O-D stretching mode (ν_{OD}) centered at ~2,500 cm^{-1} (Fig. 1*A* and *SI Appendix*, Fig. S2) of HDO diluted in H_2O. Spectral line widths of the ν_{OH} and ν_{OD} of liquid water are very broad, mainly because of the large range of H-bond strengths and strong intra- and intermolecular couplings. To measure accurately the enhancement of H-bond strength of water near hydrophobic solutes, both couplings must be eliminated. Their removal is commonly achieved by diluting a small amount of D_2O into H_2O or vice versa (23, 27). In such solutions, the H-bonded structure remains virtually unchanged. Introducing small amounts of D_2O into H_2O gives, because of H/D exchange, a mixture of predominantly HDO and H_2O in equilibrium, in which the HDO molecules are surrounded by H_2O. A mixture of 1.4% (vol/vol) D_2O in H_2O gives ~2.8% HDO, 97.2% H_2O, and only 0.02% D_2O. Because of the large differences between the frequencies of ν_{OH} and ν_{OD}, the intra- and intermolecular couplings are completely removed. The spectrum of ν_{OD} of the water molecules perturbed by solute (Fig. 1 *B* and *C* and *SI Appendix*, Fig. S4) was obtained by subtracting the spectra of pure H_2O and pure, unperturbed HDO from the spectrum of the same solution containing a small amount of hydrophobic solute. This double-subtraction procedure, introduced by Lindgren and coworkers (28), was modified to account for variable cell thickness and tested thoroughly using pure solvent (2.8% HDO in H_2O) and solutions of NaCl and methanol. The effects of temperature and pressure on the difference spectra have been investigated (*SI Appendix*). The spectra of H_2O and HDO diluted in H_2O used for subtractions were obtained at the same temperatures and pressures as the spectra of solutions of alkanes and noble gases. The same high-pressure transmission cell was used to obtain all of these spectra. To preclude formation of solid clathrates, we used pressures and temperatures positioned on the right-hand side of the equilibrium line in the pressure–temperature (PT)-phase diagram (Fig. 1*D* and *SI Appendix*).

The resulting spectra of the water molecules that are perturbed by the solutes are shown in Fig. 1 *B* and *C* and summarized in Table 1. All four solutes display a redshift of ν_{OD} ($\Delta\nu_{OD}$) of ~60 cm^{-1}, the same as those of HDO ice and HDO clathrates (Fig. 1*C* and Table 1). This observation shows that the strengths of the H bonds near purely hydrophobic solutes are enhanced to the level observed in ice and clathrates. Neither the temperature nor the pressure influence $\Delta\nu_{OD}$ significantly. The number of enhanced or ice-like H bonds per methane molecule is estimated to be between 10 and 15 (*SI Appendix*). The number of water molecules in hypothetically frozen structures is between five and eight per methane molecule. This amount is only a fraction of the number of waters in the first solvation layer of methane (i.e., 16) measured by neutron scattering (11). Our estimated number is in good agreement with the number obtained by Kauzmann (7). He estimated that, if icebergs around a methane molecule in solution are highly crystalline, they must contain less than half a dozen water molecules (7).

The line widths H_w of ν_{OD} of the water molecules perturbed by hydrophobic solutes are only slightly larger than those of clathrates

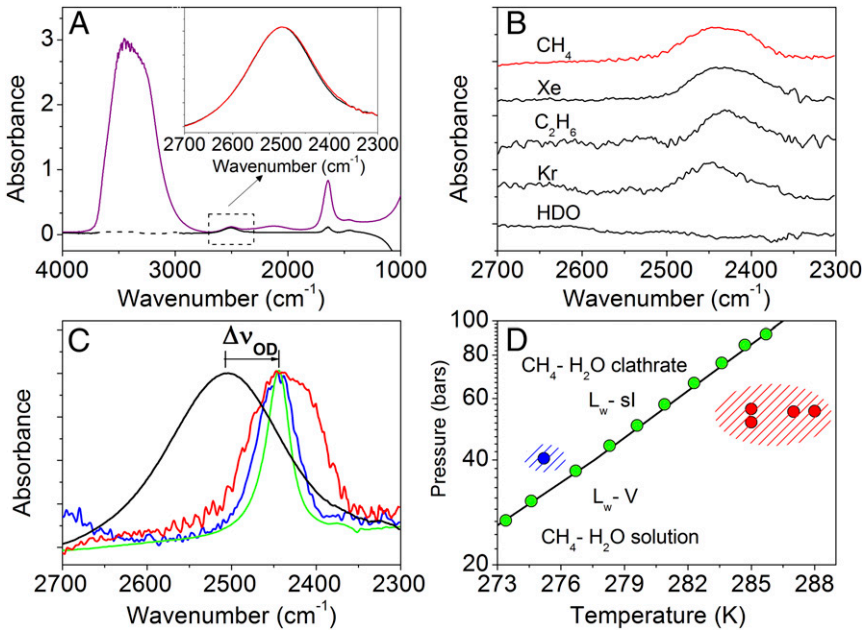

Fig. 1. Experimental data of aqueous solutions of methane, ethane, krypton, and xenon. (*A*) The purple line represents the IR spectrum of the solvent mixture (2.8% HDO in H_2O). The black line represents the spectrum of the pure unperturbed HDO molecules obtained by subtracting the spectrum of pure H_2O from the spectrum of the solvent mixture recorded under the same conditions. *Inset* shows the region of interest—the decoupled O-D stretching mode (ν_{OD}). The black line represents the ν_{OD} of the pure unperturbed HDO molecules. The red line represents the ν_{OD} of the perturbed and unperturbed HDO molecules of the solution containing a small amount of methane. (*B*) Spectra of the ν_{OD} of the HDO molecules perturbed by methane, ethane, xenon, and krypton. (*C*) Comparison of the spectra of the ν_{OD} region: liquid HDO in H_2O (293 K and 1 bar; black), perturbed HDO molecules in the methane solution (red), methane HDO clathrate (blue), and HDO ice (green). The spectra are normalized to the same height. (*D*) Phase *PT* diagram of the equilibrium between solid methane clathrate and methane aqueous solution [circles (62) and line (63)]. The red circles show the positions of four measurements used to obtain spectra of methane solutions. The blue circle shows the position of solid methane clathrate used to obtain the spectrum in *C*.

Table 1. Spectral parameters of the ν_{OD} of liquid solvent, solutions of gases, NaCl solution, clathrates, and ice

Sample	T	p	ν_{OD}	$\Delta\nu_{OD}$	H_w
Pure solvent*	293	1	2,502 (±1)	0	164 (±2)
Pure solvent*	293	56	2,502 (±1)	0 (±2)	160 (±2)
Pure solvent*	285	1	2,498 (±1)	4 (±2)	158 (±2)
Pure solvent*	285	56	2,498 (±1)	4 (±2)	158 (±2)
CH_4 solution†	285	56	2,445 (±5)	57 (±8)	92 (±8)
C_2H_5 solution†	291	14	2,430 (±5)	78 (±8)	86 (±8)
Xe solution†	299	16	2,442 (±5)	60 (±8)	96 (±8)
Kr solution†	289	50	2,445 (±5)	57 (±8)	87 (±8)
NaCl solution‡	285	53	2,536 (±5)	−34 (±8)	166 (±8)
CH_4 clathrate§	275	40	2,446 (±1)	56 (±2)	60 (±2)
C_2H_5 clathrate§	276	7	2,442 (±1)¶	60 (±2)	80 (±2)
Xe clathrate§	292	18	2,442 (±1)	60 (±2)	79 (±2)
Kr clathrate§	274	56	2,446 (±1)	56 (±2)	55 (±2)
Ice I_h	271	1	2,445 (±1)	57 (±2)	37 (±2)

Temperature T (Kelvin), pressure p (bar), frequency at maximum intensity ν_{OD} (centimeters^{-1}), frequency redshift $\Delta\nu_{OD}$ (centimeters^{-1}), and half-width H_w (centimeters^{-1}) are shown. H_w is defined as the width of a peak at one-half height. Errors in measuring T and p are estimated at 0.5 K and 0.5 bars, respectively. All samples contain a solvent mixture of 2.8% HDO in H_2O.
*Solvent mixture (2.8% HDO in H_2O) under four different conditions.
†Spectral parameters of the water molecules perturbed by solutes (Fig. 1*B*).
‡Solution of 0.03 M NaCl used for verification of the subtraction procedure (*SI Appendix*, Figs. S4 and S6). Note that the H_w of its ν_{OD} is equal to that of liquid solvent.
§Solid state (*SI Appendix*, Fig. S3).
¶Shoulder at 2,472 (±1) cm^{-1}.

and much smaller than those of the liquid solvent (Fig. 1*C* and Table 1). Temperature and pressure do not influence H_w significantly (by <6 cm^{-1}) (Table 1). Similarity of the values of H_w of the water molecules perturbed by hydrophobic solutes and those of clathrates indicates a relatively small range of H-bond strengths and thus, similar structural ordering of water molecules near the strengthened H bonds. H_w reflects structural ordering of only those water molecules that are close enough to influence values of ν_{OD}. Auer et al. (23) found that ν_{OD} of an H-bonded water pair is affected predominantly by the water molecules that are closer than 4 Å away from the tagged H-bonded atom. This local environment of an ice-like H bond consists of a water pair and approximately six nearest neighbor H-bonded water molecules arranged in two fused tetrahedrons. It should be noted that the formation of an ordered local environment around individual ice-like H bonds is quite different from the creation of fully formed clathrate-like clusters of water molecules because of the relatively small number of ice-like H bonds per single-methane molecule (see above). The ice-like H bonds may be isolated in the solvation layer, or they may merge into larger arrays to form clathrate-like structures. The extent of this fusion is unclear.

Ab Initio MD Simulations of Purely Hydrophobic Solute in Water. The results so far obtained by Monte Carlo and MD simulations of purely hydrophobic molecules in water are inconsistent. Although some simulations confirm enhanced H bonding near apolar molecules and support the iceberg view (29–31), others do not (32–36).

Ab initio MD simulations currently provide the most accurate approach to addressing the structural and dynamic aspects of water–water H bonding in a condensed phase under ambient conditions, because in these methods, the interatomic forces are derived on the fly at the quantum mechanical level. Such simulations can explicitly capture electronic polarization effects and account for the proper response of water molecules to the local environment. We performed ab initio MD simulations of methane in D_2O at three temperatures (283, 293, and 300 K) using the dispersion-corrected density functional theory (DFT) approach as implemented in the program package VASP, version 5.3 (37) (*Materials and Methods* and *SI Appendix*). The most appropriate choice of exchange-correlation functional was found to be revPBE (38, 39) in combination with the Grimme D3 correction (40), which was shown in a series of test simulations of bulk water according to the ability to best reproduce experimental radial distribution functions, diffusion constants, line shape of ν_{OD}, and solvation enthalpy of liquid water at ambient conditions (*SI Appendix*). Time-dependent O-D stretching frequencies of individual water molecules were derived using the wavelet transform of the corresponding O-D distance time series (*Materials and Methods*).

Our analysis was focused on comparing the structural and energetic properties of the H-bond network of water molecules in the immediate vicinity of methane and relative to those of bulk water (Fig. 2). The ν_{OD} frequencies as a function of distance to methane (Fig. 2*A*) clearly show notable depressions in the region of the first hydration shell. The redshifts range from 14 to 7 cm^{-1} with increasing temperature. Note, however, that the redshifts obtained by the ab initio MD simulations are not directly comparable with the experimental redshift (~60 cm^{-1}) (*SI Appendix*). Furthermore, we have analyzed the electrostatic interaction energies of water molecule pairs located in either the methane hydration layer or the bulk water. The electrostatic interaction potentials of water molecule pairs located in the methane hydration layer are consistently lower than those in the bulk water, indicating higher H-bond strength (Fig. 2*B*). The difference between hydration and bulk water pairs (Fig. 2*B*) shows clearly that the first four nearest water molecules surrounding a water molecule located in the first hydration shell around the methane interact more strongly with the tagged water molecule (by 0.1–0.15 kcal/mol) than molecules in bulk water, whereas the difference for the more distant neighbors (fifth onward) becomes negligible. This result shows that the structure of water is tetrahedral (four neighbors). The number of H bonds per water molecule and the tetrahedrality (Fig. 2 *C* and *D* and *SI Appendix*), both as a function of distance to the methane, indicate that water H bonds in the hydration shell are more numerous and more

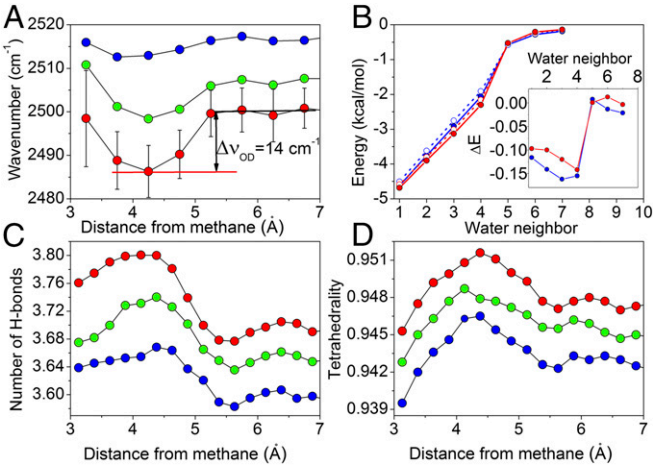

Fig. 2. Ab initio MD properties of water molecules at different temperatures as a function of their proximity to methane. Red, green, and blue colors correspond to temperatures 283, 293, and 300 K in all four panels. (*A*) O-D stretching frequency as a function of distance of water (oxygen) to methane (carbon). (*B*) Electrostatic interaction potential of water pairs at increasing intermolecular spacing sorted into a list of sequential neighbors relative to the tagged water molecule located in either the methane hydration layer (solid line) or the bulk (dashed line). The differences between hydration and bulk pair interaction potentials (kilocalories per mole) are shown in *Inset*. (*C*) Average number of H bonds per water molecule as functions of distance to methane. (*D*) Tetrahedrality as functions of distance to methane.

tetrahedrally oriented than those in bulk water. Other structural and energy parameters that characterize H-bond strength are consistent with the results presented above (*SI Appendix*, Fig. S12). The correlation times, calculated by the ab initio MD simulations, show restricted orientational mobility of the water molecules near a methane solute (*SI Appendix*, Fig. S13), in accord with the NMR data from the work by Haselmeier et al. (8). The O-D vibrational redshift, the tetrahedrality, and the number of H bonds are larger at lower temperatures.

The simulations performed in this work clearly show that water molecules in the vicinity of methane have stronger, more numerous, and more tetrahedrally oriented H bonds than those in bulk water and that their mobility is restricted, which is consistent with the experimental results presented above.

Origin of Strengthened Water H Bonds near Hydrophobic Solutes. The results presented above show that the water H bonds in the neighborhood of purely hydrophobic solutes are as strong as those in ice or clathrates. These ice-like H bonds cause greater water ordering because of formation of icebergs as postulated by Kauzmann (7). Determining the physical origin of ice-like H bonds near hydrophobic solutes is, therefore, crucial for understanding hydrophobicity at the most fundamental level. Theoretical simulations show that water H bonds straddle small hydrophobic solutes in a way similar to that of H bonds in clathrates to maximize the number of H bonds (33). Such a constraint imposed on the H-bonding network can cause ordering of water molecules per se; however, it does not necessarily make H bonds stronger. The absence of a clear connection between steric constraint and H-bond strength led us to focus on electrostatic interactions, because water H bonds are predominantly electrostatic in nature (41). H bonds in water are known to be strongly cooperative (23, 42–44); their strength, therefore, depends on electrostatic interactions of an H-bonded pair with neighboring water molecules.

We, therefore, analyzed the effects of neighboring water molecules on the strength of the H bond between a pair of waters (Fig. 3*A*, yellow) during ab initio MD simulations. It has been shown that the instantaneous frequency, ν_{OH}, is proportional to the projection of an electric field on an H atom along the bond vector O-H ($E_{O\text{-}H}$) (23, 25, 45). The electric field on an H atom depends on the positions, orientation, and point atomic charges of water molecules in the vicinity. To verify this relationship, we calculated the electric field on D atoms using the Hirshfeld's point atomic charges (46) and the corresponding frequencies of the O-D stretching mode ν_{OD} for short segments of the ab initio MD trajectory using the continuous wavelet transformation method (47). A remarkably simple linear relationship is seen to exist between the ν_{OD} frequency (i.e., H-bond strength) and the projection of the electric field along the H-bond vector D···O ($E_{D\ldots O}$) (Fig. 3*A*). We used here the values of $E_{D\ldots O}$ instead of $E_{O\text{-}D}$, because the H bonds in liquid water are rarely collinear (average angle O-D···O is 167°). The linear relation between $E_{D\ldots O}$ and ν_{OD} is crucial to our analysis, because it enables the contribution of each neighboring water molecule to the H-bond strength to be evaluated. The strength of an H bond is enhanced if a larger force propels a positively charged atom D toward an acceptor O atom. The water molecules that are closest to the donor atom D make the largest contributions to $E_{D\ldots O}$. The ν_{OD} of an H-bonded water pair is affected predominantly by water molecules in the first solvation layer (cutoff < 5 Å) (Fig. 3*B*).

Three distinct classes of water molecule (Fig. 3*B*) were identified in the neighborhood of a water H-bond pair in liquid water. The first two classes comprise the water molecules that are H-bonded to the H-bonded pair; their contributions to the value of $E_{D\ldots O}$ do not differ significantly from the contributions of the corresponding waters in ice. In ice, a pair of H-bonded water molecules is H-bonded to six water molecules located at the vertices of two fused tetrahedrons (Fig. 3*C*). In liquid water, the locations of H-bonded waters resemble fused tetrahedrons (Fig. 3*D*); however, some

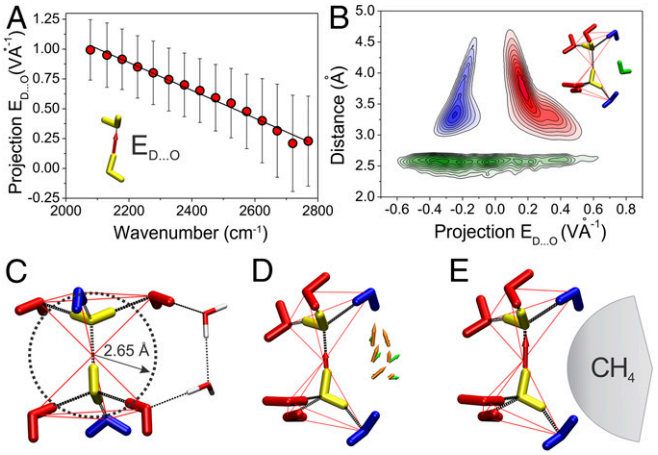

Fig. 3. Screening of a water H bond by an intercalating water molecule. (*A*) Frequency of ν_{OD} as a function of projection of electric field $E_{D\ldots O}$. Contributions of the H-bonded pair (yellow) to $E_{D\ldots O}$ are ignored. (*B*) Distribution of water molecules as a function of distance to atom D and projection of electric field $E_{D\ldots O}$. Red, blue, green, and yellow systematically correspond to classes I and II, intercalating waters, and the monitored H-bonded water pair, respectively. Class I and II waters are located on the vertices of two fused tetrahedrons. (*C*) The environment of two H-bonded waters in ice. Waters centered on the vertices of tetrahedrons are marked by red or blue depending on their class. The circle shows the cutoff distance for intercalating waters. (*D*) The environment of the two H-bonded waters in bulk liquid water. Average electric field vectors and dipole moments for intercalating waters are shown as orange and green arrows, respectively. The resulting $E_{D\ldots O}$ is shown as a red arrow. To accommodate the intercalating water molecule, the angle O-D···O of the H-bonded pair must bend. Only ~6% of the H-bonded pairs in the bulk water have intercalating waters. (*E*) The environment of the two H-bonded waters in the first solvation layer of methane. Intercalating water molecules are replaced by methane—the resulting $E_{D\ldots O}$ is larger than that of bulk water (red arrow).

vertices are empty or overpopulated. The contributions of the first two classes of water molecules to the value of $E_{D\ldots O}$ are determined primarily by the point atomic charges of atoms that are closest to the atom D of the H-bonded pair controlled by donor or acceptor characters of the corresponding H bonds. The first class is the H bond-enhancing water molecules, which increase the value of $E_{D\ldots O}$ (Fig. 3*B*, red). The second class is the H bond-weakening waters, which decrease $E_{D\ldots O}$ (Fig. 3*B*, blue). The average numbers of these two classes per H bond are 3.4 and 1.7; therefore, the net effect is to strengthen the H bond. In ice, the corresponding numbers are four and two.

The most interesting is the third class of intercalating water molecules. They are able to occupy transiently the space closest to the atom D of the H-bonded pair, which is empty in ice (Fig. 3*B*, green). To accommodate the intercalating water molecule, the angle O-D···O of the H-bonded pair must bend (Fig. 3*D*). Only ~6% of the H-bonded pairs in the bulk water (at cutoff of 2.65 Å) have intercalating waters. The intercalating waters represent a subgroup of the so-called fifth, interstitial, nontetrahedral, or mismatched water molecules (29, 48–50) that interact with the tagged water molecule by, predominantly, van der Waals forces. These water molecules are specific for liquid water and absent in ice. The intercalating water molecules are not directly H-bonded to the H-bonded pair; therefore, they have less negative solvation energy than the bulk water. The orientation and thus, also, the contribution of these water molecules to the value of $E_{D\ldots O}$ are determined mainly by the electric field generated by the first two classes. Fig. 3*D* shows that the average dipole moments of the intercalating waters are oriented in the direction of the average local electric field (Fig. 3*E*). The intercalating waters screen (shield) this electric field. Consequently, the contributions of the intercalating water molecules to $E_{D\ldots O}$ are generally negative (Fig. 3*B*, green) and

primarily responsible for the lower strength of H bonds in liquid water than those in ice.

In the transfer of the H-bonded pair from the bulk to the first solvation layer of methane (Fig. 3*E*), the fraction of intercalating water molecules per H-bonded pair is reduced from 6 to 2%, because methane and intercalating water molecules tend to occupy the same space lateral to the direction of H bonds (Fig. 3 *D* and *E*). Methane prefers this position, because water H bonds tend to straddle small hydrophobic solutes in a way similar to that in clathrates. By removing the intercalating water molecules, the value of $E_{D\ldots O}$ increases. A higher value of the projection of electric field $E_{D\ldots O}$ means that a larger force is pushing a positively charged D atom toward the acceptor O atom, which strengthens the H bond. This mechanism explains why water H bonds near methane are stronger than those in bulk water.

The explanation described above for the strengthening of water H bonds near hydrophobic solutes is in accord with the general concept that electrostatic interactions are stronger near hydrophobic groups. Berry and coworkers (51) have shown that water molecules in the neighborhood of a hydrophobic solute have a smaller dielectric susceptibility or in microscopic terms, less effective electrostatic screening (52). It has been shown that electrostatic screening is the main reason for the distinct backbone conformational preferences of amino acid residues in peptides and proteins (53), the nearest neighbor effect (54), and the formation of transient β-strands in unfolded proteins (55). It has also been shown, using amide to ester mutations, that H bonds in the protein interior are stronger than those exposed to solvent (56–58).

Conclusion

By applying methods of superior accuracy for measuring and calculating subtle effects of H-bonding in water, we have obtained evidence that supports, unequivocally, the iceberg view of hydrophobicity proposed by Frank and Evans (6) and Kauzmann (7). Our experimental results show that water H bonds near purely hydrophobic solutes are strengthened to the level observed in ice and clathrates. We have proposed a physical origin for hydrophobicity based on electrostatic screening that couples hydrophobic with electrostatic interactions. This coupling may be crucial in understanding protein folding and other complex phenomena.

Materials and Methods

Materials. Samples were prepared using milli-Q H_2O and D_2O (Euriso top, 99.90% D). Gases used were methane (Messer, 4.5), ethane (Messer, 3.5), krypton (Messer, 3.0), and xenon (Messer, 5.0).

Instruments and Sample Preparation. IR spectra were recorded on Bruker Vertex 80 and Tensor 27 Spectrometers and collected in the transmission mode with a nominal resolution of 4 cm^{-1}. Typically, 128 interferograms were averaged and apodized using the Gapp–Henzel function. A deuterated triglycine sulphate (DTGS) detector was used throughout. The aperture of the IR beam was set to values between 2 and 4 mm. A Harrick (HPL-TC-13-3) high-pressure and high-temperature sample cell was used for high-pressure measurements (*SI Appendix*, Fig. S1). The errors in measuring temperature and pressure are estimated at 0.5 K and 0.5 bar, respectively.

OPUS software (Ver. 6.5) was used for subtraction of spectra. Elimination of CO_2 bands has been performed manually.

Solutions of 2.8% (by volume) HDO in H_2O were used for all IR measurements. They were prepared by mixing 1.4% D_2O and 98.6% H_2O. HDO/H_2O solution was used to eliminate inter- and intramolecular vibrational coupling and prevent saturation of the O-D stretching mode by significantly reducing its intensity. The small amount of HDO in H_2O ensures that intensities of the O-D stretching peak are below saturation level. The solution of 2.8% HDO in H_2O is a compromise between factors that govern band saturation (i.e., dynamic range of the fully decoupled O-D stretching mode and subtraction of the H_2O combination band). Spectra of pure H_2O were recorded at the same temperatures and pressures as those for the solutions.

Ab Initio MD Simulations. The ab initio MD simulations were performed using the Vienna Ab Initio Simulation Package (VASP, version 5.3) (37). This code, one of the fastest ab initio computer packages available, combines plane-wave implementation of the DFT in combination with the projector-augmented wave (PAW) pseudopotential (59). In general, the PAW pseudopotential is more accurate than the ultrasoft pseudopotential, because it provides an exact valence wave function in the core region of the electron orbital.

The molecular systems were constructed at three different temperatures (283, 293, and 300 K) by inserting one methane molecule per cubic box containing 91 D_2O molecules. Sizes of simulation cells were set according to the experimental densities of liquid water at three corresponding temperatures, assuming that the volume of one methane molecule occupies approximately the volume of two water molecules. Accordingly, three cubic boxes of sizes 14.06605, 14.07299, and 14.08090 Å were used for the simulations at 283, 293, and 300 K, respectively. The initial molecular setup was achieved by running short classical MD simulations in the microcanonical (NVE) ensembles using the TIP4P/2005 water model (60) with methane parameters introduced by Docherty et al. (61). This step was followed by extensive ab initio MD simulations, in which each system was first equilibrated for 100 ps and simulated further for 250 ps at 283 and 293 K and 100 ps at 300 K to produce corresponding canonical (NVT) ensembles for analysis. Shorter (100 ps) control MD runs were performed at slightly increased and decreased densities by varying the size of the simulation box by ±1% to explore the effect of pressure on the results.

Simulated trajectories were saved every 1 fs and used for structural and O-D stretching vibrational analyses. The O-D stretching vibrational spectrum was calculated based on continuous wavelet transformation of the trajectories as introduced by Vela-Arevalo and Wiggins (47). The vibrational frequency of an individual O-D bond at a given moment is obtained through a time series analysis of the O-D distance. This approach enabled position- and time-dependent O-D frequencies to be obtained, which could be correlated with the structural and dynamic properties of the H-bonded network. The point atomic charges used to calculate electric fields were calculated from the instant electron density of the system according to the Hirshfeld definition (46).

ACKNOWLEDGMENTS. We thank R. Pain, J. Moult, K. Dill, R. L. Baldwin, and B. K. Lee for critical discussions and reading of the manuscript and G. Bercic and I. Vovk for support in the high-pressure experiments. This work was funded by Slovenian Research Agency Grants P1-0010 and J1-7441 and Excellent NMR - Future Innovation for Sustainable Technologies (ENFIST) Centre of Excellence.

1. Blokzijl W, Engberts JBFN (1993) Hydrophobic effects - opinions and facts. *Angew Chem Int Ed Engl* 32(11):1545–1579.
2. Southall NT, Dill KA, Haymet ADJ (2002) A view of the hydrophobic effect. *J Phys Chem B* 106(3):521–533.
3. Dill KA, Truskett TM, Vlachy V, Hribar-Lee B (2005) Modeling water, the hydrophobic effect, and ion solvation. *Annu Rev Biophys Biomol Struct* 34:173–199.
4. Ball P (2008) Water as an active constituent in cell biology. *Chem Rev* 108(1):74–108.
5. Laage D, Stirnemann G, Sterpone F, Rey R, Hynes JT (2011) Reorientation and allied dynamics in water and aqueous solutions. *Annu Rev Phys Chem* 62:395–416.
6. Frank HS, Evans MW (1945) Free volume and entropy in condensed systems III. Entropy in binary liquid mixtures; partial molal entropy in dilute solutions; structure and thermodynamics in aqueous electrolytes. *J Chem Phys* 13(11):507–532.
7. Kauzmann W (1959) Some factors in the interpretation of protein denaturation. *Adv Protein Chem* 14:1–63.
8. Haselmeier R, Holz M, Marbach W, Weingartner H (1995) Water dynamics near a dissolved noble-gas - first direct experimental-evidence for a retardation effect. *J Phys Chem-Us* 99(8):2243–2246.
9. Muller N (1990) Search for a realistic view of hydrophobic effects. *Acc Chem Res* 23(1):23–28.
10. Nemethy G, Scheraga HA (1962) Structure of water and hydrophobic bonding in proteins. II. Model for the thermodynamic properties of aqueous solutions of hydrocarbons. *J Chem Phys* 36(12):3401–3417.
11. Koh CA, Wisbey RP, Wu XP, Westacott RE, Soper AK (2000) Water ordering around methane during hydrate formation. *J Chem Phys* 113(15):6390–6397.
12. Buchanan P, Aldiwan N, Soper AK, Creek JL, Koh CA (2005) Decreased structure on dissolving methane in water. *Chem Phys Lett* 415(1-3):89–93.
13. Bowron DT, Filipponi A, Lobban C, Finney JL (1998) Temperature-induced disordering of the hydrophobic hydration shell of Kr and Xe. *Chem Phys Lett* 293(1-2):33–37.
14. Stirnemann G, Hynes JT, Laage D (2010) Water hydrogen bond dynamics in aqueous solutions of amphiphiles. *J Phys Chem B* 114(8):3052–3059.
15. Ball P (2011) Biophysics: More than a bystander. *Nature* 478(7370):467–468.
16. Lee B (1985) The physical origin of the low solubility of nonpolar solutes in water. *Biopolymers* 24(5):813–823.
17. Baldwin RL (2014) Dynamic hydration shell restores Kauzmann's 1959 explanation of how the hydrophobic factor drives protein folding. *Proc Natl Acad Sci USA* 111(36):13052–13056.
18. Novak A (1974) Hydrogen bonding in solids. Correlation of spectroscopic and crystallographic data. *Struct Bonding* 18:177–216.

19. Stiopkin IV, et al. (2011) Hydrogen bonding at the water surface revealed by isotopic dilution spectroscopy. *Nature* 474(7350):192–195.
20. Hecht D, Tadesse L, Walters L (1992) Defining hydrophobicity - probing the structure of solute-induced hydration shells by fourier-transform infrared-spectroscopy. *J Am Chem Soc* 114(11):4336–4339.
21. Hecht D, Tadesse L, Walters L (1993) Correlating hydration shell structure with amino-acid hydrophobicity. *J Am Chem Soc* 115(8):3336–3337.
22. Sharp KA, Madan B, Manas E, Vanderkooi JM (2001) Water structure changes induced by hydrophobic and polar solutes revealed by simulations and infrared spectroscopy. *J Chem Phys* 114(4):1791–1796.
23. Auer B, Kumar R, Schmidt JR, Skinner JL (2007) Hydrogen bonding and Raman, IR, and 2D-IR spectroscopy of dilute HOD in liquid D2O. *Proc Natl Acad Sci USA* 104(36):14215–14220.
24. Davis JG, Gierszal KP, Wang P, Ben-Amotz D (2012) Water structural transformation at molecular hydrophobic interfaces. *Nature* 491(7425):582–585.
25. Hamm P, Zanni MT (2011) *Concepts and Methods of 2D Infrared Spectroscopy* (Cambridge Univ Press, Cambridge, UK).
26. Laage D, Stirnemann G, Hynes JT (2009) Why water reorientation slows without iceberg formation around hydrophobic solutes. *J Phys Chem B* 113(8):2428–2435.
27. Falk M, Ford TA (1966) Infrared spectrum and structure of liquid water. *Can J Chem* 44:1699–1707.
28. Bergstrom PA, Lindgren J, Kristiansson O (1991) An IR study of the hydration of $ClO4^-$, NO_3^-, I^-, Br^-, Cl^-, and SO_4^{2-} anions in aqueous-solution. *J Phys Chem-Us* 95(22): 8575–8580.
29. Sharp KA, Madan B (1997) Hydrophobic effect, water structure, and heat capacity changes. *J Phys Chem B* 101(21):4343–4348.
30. Raschke TM, Levitt M (2005) Nonpolar solutes enhance water structure within hydration shells while reducing interactions between them. *Proc Natl Acad Sci USA* 102(19): 6777–6782.
31. Titantah JT, Karttunen M (2012) Long-time correlations and hydrophobe-modified hydrogen-bonding dynamics in hydrophobic hydration. *J Am Chem Soc* 134(22):9362–9368.
32. Kirchner B, Stubbs J, Marx D (2002) Fast anomalous diffusion of small hydrophobic species in water. *Phys Rev Lett* 89(21):215901.
33. Montagna M, Sterpone F, Guidoni L (2012) Structural and spectroscopic properties of water around small hydrophobic solutes. *J Phys Chem B* 116(38):11695–11700.
34. Godec A, Smith JC, Merzel F (2011) Increase of both order and disorder in the first hydration shell with increasing solute polarity. *Phys Rev Lett* 107(26):267801.
35. Godec A, Merzel F (2012) Physical origin underlying the entropy loss upon hydrophobic hydration. *J Am Chem Soc* 134(42):17574–17581.
36. Godec A, Smith JC, Merzel F (2013) Soft collective fluctuations governing hydrophobic association. *Phys Rev Lett* 111(12):127801.
37. Kresse G, Hafner J (1993) Ab initio molecular dynamics for liquid metals. *Phys Rev B Condens Matter* 47(1):558–561.
38. Zhang YK, Yang WT (1998) Comment on "Generalized gradient approximation made simple." *Phys Rev Lett* 80(4):890.
39. Perdew JP, Burke K, Ernzerhof M (1996) Generalized gradient approximation made simple. *Phys Rev Lett* 77(18):3865–3868.
40. Grimme S, Antony J, Ehrlich S, Krieg H (2010) A consistent and accurate ab initio parametrization of density functional dispersion correction (DFT-D) for the 94 elements H-Pu. *J Chem Phys* 132(15):154104.
41. Mitchell JBO, Price SL (1990) The nature of the N-H O=C hydrogen-bond - an intermolecular perturbation-theory study of the formamide formaldehyde complex. *J Comput Chem* 11(10):1217–1233.
42. Dannenberg JJ (2002) Cooperativity in hydrogen bonded aggregates. Models for crystals and peptides. *J Mol Struct* 615(1-3):219–226.
43. Bartha F, Kapuy O, Kozmutza C, Van Alsenoy C (2003) Analysis of weakly bound structures: Hydrogen bond and the electron density in a water dimer. *J Mol Struc-Theochem* 666:117–122.
44. Ohno K, Okimura M, Akai N, Katsumoto Y (2005) The effect of cooperative hydrogen bonding on the OH stretching-band shift for water clusters studied by matrix-isolation infrared spectroscopy and density functional theory. *Phys Chem Chem Phys* 7(16):3005–3014.
45. Fecko CJ, Eaves JD, Loparo JJ, Tokmakoff A, Geissler PL (2003) Ultrafast hydrogen-bond dynamics in the infrared spectroscopy of water. *Science* 301(5640):1698–1702.
46. Hirshfeld FL (1977) Bonded-atom fragments for describing molecular charge-densities. *Theor Chim Acta* 44(2):129–138.
47. Vela-Arevalo LV, Wiggins S (2001) Time-frequency analysis of classical trajectories of polyatomic molecules. *Int J Bifurcat Chaos* 11(5):1359–1380.
48. Eisenberg D, Kauzmann W (1969) *The Structure and Properties of Water* (Oxford Univ Press, Oxford).
49. Sciortino F, Geiger A, Stanley HE (1991) Effect of defects on molecular mobility in liquid water. *Nature* 354(6350):218–221.
50. Kusalik PG, Svishchev IM (1994) The spatial structure in liquid water. *Science* 265(5176):1219–1221.
51. Despa F, Fernández A, Berry RS (2004) Dielectric modulation of biological water. *Phys Rev Lett* 93(22):228104.
52. Warshel A, Russell ST (1984) Calculations of electrostatic interactions in biological systems and in solutions. *Q Rev Biophys* 17(3):283–422.
53. Avbelj F, Moult J (1995) Role of electrostatic screening in determining protein main chain conformational preferences. *Biochemistry* 34(3):755–764.
54. Avbelj F, Baldwin RL (2004) Origin of the neighboring residue effect on peptide backbone conformation. *Proc Natl Acad Sci USA* 101(30):10967–10972.
55. Avbelj F, Grdadolnik SG (2007) Electrostatic screening and backbone preferences of amino acid residues in urea-denatured ubiquitin. *Protein Sci* 16(2):273–284.
56. Deechongkit S, Dawson PE, Kelly JW (2004) Toward assessing the position-dependent contributions of backbone hydrogen bonding to beta-sheet folding thermodynamics employing amide-to-ester perturbations. *J Am Chem Soc* 126(51):16762–16771.
57. Wang M, Wales TE, Fitzgerald MC (2006) Conserved thermodynamic contributions of backbone hydrogen bonds in a protein fold. *Proc Natl Acad Sci USA* 103(8):2600–2604.
58. Gao J, Bosco DA, Powers ET, Kelly JW (2009) Localized thermodynamic coupling between hydrogen bonding and microenvironment polarity substantially stabilizes proteins. *Nat Struct Mol Biol* 16(7):684–690.
59. Kresse G, Joubert D (1999) From ultrasoft pseudopotentials to the projector augmented-wave method. *Phys Rev B* 59(3):1758–1775.
60. Abascal JLF, Vega C (2005) A general purpose model for the condensed phases of water: TIP4P/2005. *J Chem Phys* 123(23):234505.
61. Docherty H, Galindo A, Vega C, Sanz E (2006) A potential model for methane in water describing correctly the solubility of the gas and the properties of the methane hydrate. *J Chem Phys* 125(7):074510.
62. Ballard AL, Sloan ED (2001) Hydrate phase diagrams for methane plus ethane plus propane mixtures. *Chem Eng Sci* 56(24):6883–6895.
63. Adisasmito S, Frank RJ, Sloan ED (1991) Hydrates of carbon-dioxide and methane mixtures. *J Chem Eng Data* 36(1):68–71.